



SAKARYA ÜNİVERSİTESİ

FEN BİLİMLERİ ENSTİTÜSÜ DERGİSİ

Sakarya University Journal of Science
SAUJS

ISSN 1301-4048 e-ISSN 2147-835X Period Bimonthly Founded 1997 Publisher Sakarya University
<http://www.saujs.sakarya.edu.tr/>

Title: Multilayer Flexible SU8-Gold Microelectrode Arrays for Wearable Bioelectronics

Authors: Murat Kaya YAPICI

Received: 2022-04-23 00:00:00

Accepted: 2022-11-21 00:00:00

Article Type: Research Article

Volume: 27

Issue: 1

Month: February

Year: 2023

Pages: 55-66

How to cite

Murat Kaya YAPICI; (2023), Multilayer Flexible SU8-Gold Microelectrode Arrays for Wearable Bioelectronics. Sakarya University Journal of Science, 27(1), 55-66, DOI: 10.16984/saufenbilder.1108035

Access link

<https://dergipark.org.tr/en/pub/saufenbilder/issue/75859/1108035>

New submission to SAUJS

<http://dergipark.gov.tr/journal/1115/submission/start>

conventional silver/silver chloride (Ag/AgCl) electrodes is critical.

Ag/AgCl electrodes, otherwise referred to as “wet electrodes”, are the gold standard in electrophysiology and the default choice especially in clinical settings. However, the existence of a gel layer in wet electrodes is known to cause skin irritation and user discomfort [10], which prohibit the use of conventional electrodes in emerging application areas like the internet of healthcare things (IoHT) where wearability and/or skin compatibility are important features of the electrode and affect the overall system performance. Similarly, the miniaturization and controlled, scalable fabrication of electrodes with varying dimensions and geometries which permit direct interfacing with readout electronics to enable system-level integration is yet another source of motivation towards the development of flexible bioelectrodes.

To address these issues, several attempts have been made to realize gel-free, skin conformal bioelectrodes including electronic tattoos [11], conductive textiles [12], polymers that are either doped with conductive ingredients (nanoparticles, conductive polymers) [13] or those that are coated or printed with electroconductive thin film layers [14].

One very critical aspect for the stated application areas which is often times overlooked is, the actual interfacing of contact electrodes with readout electronics [15]. Typically, the electrode structure has an “active”, electrically conductive side and the remainder of the structure is passivated usually by a polymeric layer which at the same time provides mechanical stability to the electrode. In actual use, active region (bottom side) of the bioelectrode is placed in direct contact with the skin and the signal is routed out from the other end (top side) by thick, metallic snap connectors or flex connectors. However, such connectors are not suitable in cases when the electrode

entails a skin-conformal design with the electrode support layer (backing) made up of thin biodegradable polymers, as in the case of electronic skin patches [16]. Therefore, there is always a need to interface the electrode to external readout circuitry and excluding the few inductive coupling approaches [17], this is usually achieved through physical wiring at the expense of skin-electrode conformality and wearability.

In this work, a tri-layer polymer-metal-polymer microelectrode architecture is demonstrated which can be readily interfaced with readout electronics. Owing to the novel design and process technology reported herein, contact pads were placed at the top side of the electrode at an elevation higher than the skin which provided robust electrical routing without disturbing the skin-electrode interface. The unique fabrication approach developed in this work allows sandwiching of thin film gold (Au) in between polymeric SU-8 layers to achieve flexible microelectrodes with arrayed sensing nodes on the bottom side of the electrode to conform to skin. Meanwhile, electrical contact pads are realized on the top side of the electrode through metal deposition on SU-8 trenches with positively inclined sidewalls. The microfabrication process is optimized to achieve high yields, and functionality of the flexible microelectrodes were demonstrated by successful recording of cardiac biopotentials.

2. MICROFABRICATION OF FLEXIBLE MICROELECTRODES

Schematic view of the multilayer flexible microelectrode array in polymer-metal-polymer sandwich structure is shown in Fig. 1. Herein, the concept is to squeeze thin-film metal traces in between photo-patternable epoxy layers, to realize a composite microelectrode structure with accurate control on the contact size, density and locations of the sensing nodes.

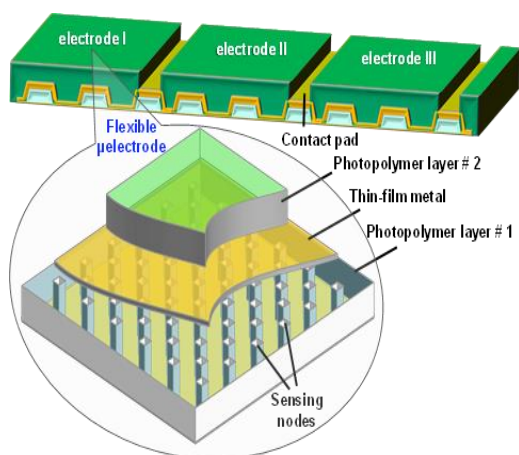


Figure 1 Schematic of the flexible microelectrode design

The microfabrication of flexible microelectrodes starts with the optimization of lithography conditions for photo-patternable epoxy layers on different substrate surfaces which is critical for successful realization of a multilayer stack.

2.1. Process Development for Patterning of SU8 on Metallic Surfaces

To realize the multilayer flexible microelectrode array, SU-8 (Kayaku Advanced Materials Inc., Westborough, MA) which is an epoxy-based negative photoresist, was selected as the photopolymer layer; owing to its widespread use in microfabrication, the ability to form stable films at wide range of film thicknesses, its chemical stability and biocompatibility [18, 19]. In the sandwich-like flexible microelectrode design (Fig. 1), SU-8 layers of two different thickness is employed, specifically “SU-8 5” on top of an aluminum (Al) sacrificial layer and “SU-8 50” atop the buried gold (Au) conductor layer.

The patterning of SU-8 even on flat silicon surface can be tricky and usually requires tight control of lithography process

parameters. Given the multilayer composite structure of the flexible microelectrode array, several experiments were performed to optimize the soft bake, post-exposure bake (PEB) and exposure parameters to ensure successful patterning.

For patterning experiments, 4 in (100) silicon wafers were cleaved into smaller samples of $\sim 2 \times 2$ cm and coated with aluminum and gold thin-film layers. First, lithography parameters for a $7 \mu\text{m}$ -thick “SU-8 5” layer on Al surface were optimized. Table 1 summarizes the different experimental conditions that were tested, where the soft bake and PEB temperature and time were varied, along with the exposure dose. For all samples, solvent cleaning and dehydration bake steps were performed prior to resist coating, and the spin speed was set according to manufacturer’s data sheet to yield the desired film thickness.

As a starting point in process optimization, SU-8 was patterned on a bare silicon sample. Upon spin coating of the SU-8 film, a two-step soft bake at 75°C for 2 min and 115°C for 5 min. was performed, followed by exposure with 365 nm UV light at a dose of 200 mJ, and a two-step PEB at 75°C for 1 min and 115°C for 3 min, after which the sample was developed long enough to clear SU-8 from all unexposed (masked) regions. The sample was inspected with an optical microscope to validate the pattern fidelity; in other words, the precision in qualitative terms (good, acceptable, or bad) with which patterns on the mask are replicated onto the wafer. Using these process parameters, it was verified that patterns could be replicated onto silicon wafer surface with good fidelity (see Sample#1 i.e., S1, in Table 1).

Table 1 “SU8-5” and “SU-8 50” lithography parameter optimization on aluminum and gold-coated silicon wafers

Sample# (surface [§])	Soft Bake (°C)	PEB (°C)	Dose (mJ)	Pattern fidelity*
S1 (Si/SU8-5)	75°C (2') 115°C (5')	75°C (1') 115°C (3')	200mJ	Good
S2 (Al/SU8-5)	75°C (2') 115°C (5')	75°C (1') 115°C (3')	200mJ	Bad
S3 (Al/SU8-5)	65°C (1') ↓ 95°C (3') ↓	65°C (1') ↓ 95°C (2'15'') ↓	200mJ –	Bad
S4 (Al/SU8-5)	65°C (2') ↓ 105°C (5') ↓	65°C (1') ↓ 95°C (1') ↓	200mJ –	Bad
S5 (Al/SU8-5)	65°C (2') ↓ 105°C (5') ↓	75°C (1') – 105°C (3') ↓	250mJ ↑	Bad
S6 (Al/SU8-5)	75°C (2') – 115°C (5') –	75°C (1') – 115°C (3') –	125mJ ↓	Bad
S7 (Al/SU8-5)	65°C (1') ↓ 95°C (3') ↓	65°C (1') ↓ 95°C (2'30'') ↓	100mJ ↓	Acceptable
S8 (Al/SU8-5)	65°C (1') ↓ 95°C (3') ↓	65°C (1') ↓ 95°C (2'30'') ↓	80mJ ↓	Good
S9 (Au/SU8-50)	65°C (5') 95°C (15')	65°C (1') 95°C (4')	135mJ	Good

* Pattern fidelity (good/acceptable/bad) indicates how accurate patterns on the mask are replicated onto the substrate after lithography. “Bad” indicates photoresist residue inside cavities and thick line edges. Arrows (↑↓) indicates increasing/decreasing the relevant parameter (temperature/time, exposure dose), while dash (–) means no change in the relevant parameter with respect to optimized conditions on Si surface (sample 1). [§] Si – Silicon, Al – Aluminum, Au – Gold

However, the same parameters resulted in poor patterning results when the silicon wafer was coated with a layer of aluminum (S2). Essentially, a periodic array of “square” trenches with dimensions in the range of 50µm-200µm that were supposed to be patterned into the SU8 layer did not clear out completely, with visible SU-8 residues remaining inside the cavities, and the entire SU-8 layer displayed severe cracks in the film. SU-8 is notorious for cracking and adhesion failure due to buildup of tensile stress in the film during baking steps because of differences in temperature coefficients of expansion between SU-8 and underlying substrate and also due to polymerization of SU-8 [20].

To address these issues, the three most critical parameters that affect lithography performance namely soft-bake and post-exposure bake (PEB) temperature and duration, and exposure dose [21], were varied to optimize the patterning of “SU-8 5” on aluminum-coated silicon wafers. First, keeping the exposure dose constant, the soft bake and post-exposure bake temperatures and durations were lowered in an effort to mitigate build-up of stress in the SU8 film during crosslinking and alleviate cracking [22]. Accordingly, the two-step soft bake and post-expose bake conditions

were adjusted such that temperatures in the soft bake and post-exposure bake steps were not allowed to exceed 105°C, and typically reduced to the 65°C to 95°C window, along with lowering either one (but not both) of the bake durations approximately by half (43% reduction in soft bake for S3, and 50% reduction in post-exposure bake for S4). The motivation here was to minimize the thermal budget as much as possible, while still providing adequate heat to facilitate solvent evaporation during soft bake and enable crosslinking of exposed SU8 during post-expose bake. However, the pattern fidelity was still bad, with residual SU-8 inside the cavities and no significant improvement in cracking was observed.

Next the exposure dose was varied along with the bake conditions. The dose was first increased to 250 mJ along with some reduction in soft bake and PEB conditions, which did not improve the patterning result (S5 in Table 1). Therefore, considering the reflectance of aluminum usually reaching 90% or above at 365 nm regime [23], the exposure dose was gradually lowered to eliminate unintended polymerization of SU-8 due to surface reflections in regions that are otherwise masked from ultraviolet exposure.

As a starting point, the bake conditions were reverted back to the optimized conditions identified for the silicon sample, and the dose was lowered down to 125 mJ, but still no discernible improvement in pattern fidelity was observed. Reducing the soft bake and PEB temperatures to 65°C to 95°C window again and the soft bake duration nearly by half, along with lowering the exposure dose gradually to 100 mJ (S7) and 80 mJ (S8) resulted in better patterning results. Accordingly, the optimal conditions for patterning “SU-8 5” on aluminum surfaces were identified as: two-step soft bake at 65°C for 1 min and 95°C for 3 min, two-step PEB at 65°C for 1 min and 95°C for 2.5 min, and exposure dose of 80 mJ.

To test the patterning of thick “SU-8 50” on Au surfaces (S9), a similar protocol was followed wherein SU-8 with a target layer thickness of ~ 50 μm was spin-coated on the substrate surface and a two-step soft-bake was performed. Compared to “SU-8 5”, the soft-bake temperatures were kept the same; however, due to the significantly thicker “SU-8 50” film, the soft-bake durations were increased to ensure solvent evaporation. Accordingly, the sample was soft-baked at 65°C for 5 min and 95°C for 15 min. Next, exposure and post-exposure bake parameters were calibrated similar to the strategy followed in the optimization of “SU-8 5”. To achieve good pattern fidelity on “SU-8 50” on Au-coated surfaces, the optimal dose was identified as 135 mJ, and two-step PEB parameters were determined as 65°C for 1 min and 95°C for 4 min.

Typical development times in SU-8 developer (i.e. 1-methoxy-2-propyl acetate or PGMEA) were identified as ~1 min. for “SU-8 5” films and ~3 min. for “SU-8 50” films. To terminate the develop step, samples were rinsed in IPA where any “white film” formation on sample surface indicated improper development and the develop time was extended. Following the rinse cycle in IPA, samples were gently blow-dried with nitrogen.

Under the optimal conditions, pattern fidelity was good, wherein, no residual SU-8 was observed inside cavities. However, surface cracks in the patterned SU-8 layer still existed both for the case of “SU-8 5” on Al surface (Fig. 2a) and “SU-8 50” on Au surface (Fig. 2b). Micro cracks in the SU-8 layer is inherently related to residual stress in the cross-linked film, and also highly dependent on pattern density and shape. It was observed that, periodic patterns with corners tend to create localized stress regions leading to higher probability of cracking. To eliminate these cracks, a “crack anneal” procedure was developed, whereby hardbaking of the SU-8 patterned substrate in a 135°C convection oven for 5 minutes allowed reflow of the SU-8 layer and effectively healed all cracks (Fig. 2c-2d). This procedure was found to be repeatable and reliable for SU-8 formulations of different thicknesses (“SU-8 5” and “SU-8 50”) as well as the different substrates (aluminum and gold) that they are coated onto.

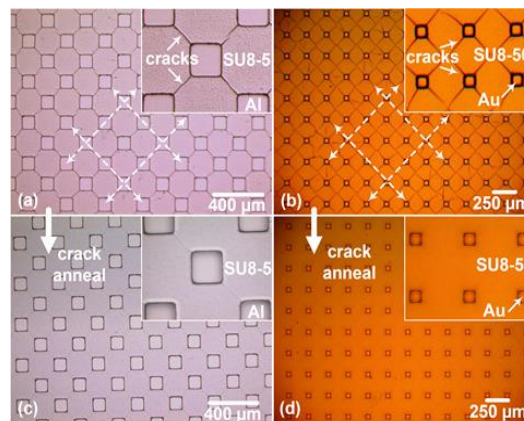


Figure 2 Optical microscope images of sample surfaces during SU8 lithography process optimization: (a)-(b) SU8-5 and SU8-50 patterns realized on Al and Au surfaces, respectively; (c)-(d) sample surfaces after the “crack anneal” step showing effective healing of cracks with thermal reflow of SU-8

2.2. Flexible Microelectrode Fabrication Process Flow

The fabrication of the flexible microelectrode begins with the deposition

of a sacrificial layer material. For this purpose, a metallic sacrificial layer, specifically aluminum (Al) was chosen. The silicon substrate was immersed into and cycled in standard solvent-based cleaning chemistry (i.e. acetone/isopropyl alcohol/distilled water/methanol) prior to physical vapor deposition in an electron beam evaporation system. A relatively slow deposition rate of ~ 0.5 nm/s was used with substrate rotation to ensure uniform thin-film Al coating with a total thickness of ~ 100 nm (Fig. 3a).

Following the deposition of the sacrificial layer material, a subsequent polymeric layer was patterned (Fig. 3b and 3c). For patterning of SU-8, first the sample was dehydrated in a convection oven at 135°C for 10 min and cooled down for 20 min prior to spin-coating of “SU-8 5” at a rate of 2000 rpm for 30s. Then, the film was patterned using the optimized parameters corresponding to Sample#8 listed in Table 1.

After this step, the process continued with the deposition of the metal layer to form the sensing electrodes. For this purpose, gold (Au) was chosen, and the deposition was performed with standard parameters at a rate of $2\text{-}3\text{\AA}/\text{s}$ in an e-beam evaporator. The thickness of the deposited metal layer was around 300 nm (Fig. 3d).

Once the metallization step was complete, a $50\ \mu\text{m}$ -thick layer of SU-8 was spin-coated and patterned on the substrate as a handle and lock-in structure (Fig. 3e and 3f). While the “SU-8 5” layer created trenches into which gold was deposited and formed the “sensing nodes”, the subsequently patterned “SU-8 50” layer filled these trenches, sandwiching the Au layer in between. This approach essentially formed a matrix of discrete sensing nodes patterned in the form of square patches at the bottom side of the microelectrode structure directly interfacing with the skin, while being electrically connected at the top side owing

to the metal coating on the sidewall of the “SU-8 5” layer acting like a via. The entire microelectrode structure resembles an array of inverted trapezoidal metallic pillars supported by two SU-8 layers.

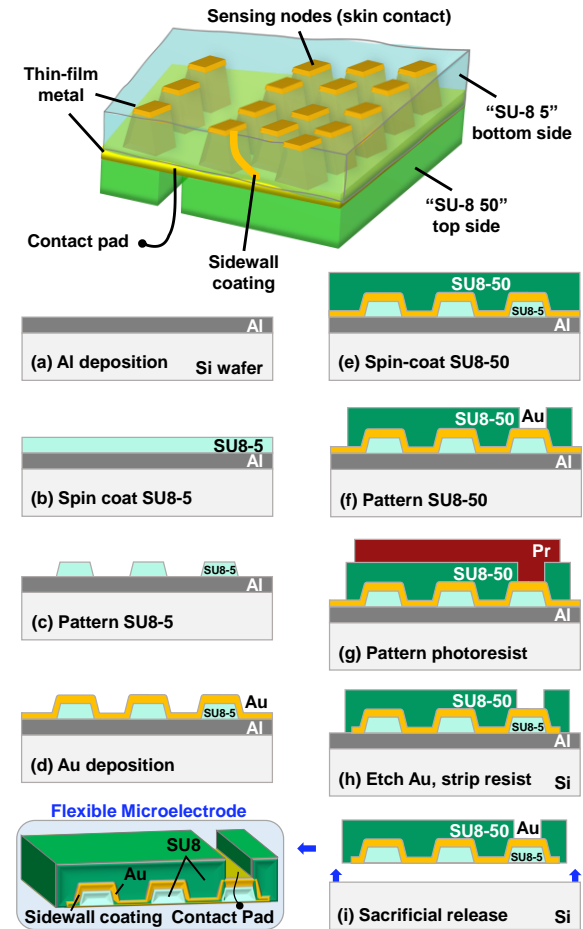


Figure 3 Perspective view and 2D-cross-sectional diagrams summarizing the process flow for microfabrication of the flexible microelectrode array

The fabrication continued with patterning of the gold layer to define the boundaries of the microelectrode, and also remove the gold inside etch holes. For this purpose, AZ 5214E photoresist (PR) was spin-coated at a rate of 4000 rpm for 30s to create $\sim 1.4\ \mu\text{m}$ -thick layer of PR coating. Next, the sample was soft-baked at 105°C for 1 min. and UV-exposed at a dose of 80 mJ and developed (Fig. 3g). To etch the gold layer, a commercial formulation based on potassium iodide (KI) was used and upon completion of Au etching, the photoresist was stripped in acetone (Fig. 3h). Finally, to

release the microelectrode structure, sacrificial layer aluminum was removed using diluted hydrochloric acid (HCL:H₂O=1:3) at room temperature.

Removal of the sacrificial layer was facilitated by etch holes that provided easy passage and penetration of the etchant solution underneath the “SU-8 5” and Au layers. Sacrificial layer etching did not cause damage to the SU8 layers or the Au structural layer, and typically within a few hours microelectrode structures could be released successfully (Fig. 3i).

2.3. Fabrication Results

Visual inspection with an optical microscope and surface profilometry measurements were performed during each step of the fabrication to ensure process control and accuracy. In Fig. 4a and 4b below, optical microscope images of the patterned “SU-8 5” layer on Al-coated substrate along with the step-height measurement is shown. The thickness of the first layer was targeted around 7 μm , and this was verified with surface profilometry measurements.

The novel microelectrode design developed in this work requires trenches to be opened in the first photopolymer layer (“SU-8 5” layer on the bottom side contacting the skin). Since e-beam evaporation produces conformal layers, deposited gold was coated everywhere on the patterned “SU-8 5” layer including the interior of the trenches as well as the sidewall and top surface of the “SU-8 5” layer. Therefore, by designing and lithographically controlling the trench dimensions in the “SU-8 5” layer and their periodicity, the contact area of an individual sensing node (e.g. 50x50 μm , 100x100 μm , and 150x150 μm) and total number of nodes in the array were controlled. Simultaneously with the sensing nodes, initial footprint of the etch holes were also successfully patterned in the “SU-8 5” layer.

Once patterning of the “SU-8 5” layer was complete, Au deposition was performed as described, and the second photopolymer layer (“SU-8 50” layer on the top side for electrical interfacing and mechanical stability) was patterned as described in the fabrication process flow. As shown in Fig. 4c inset, patterns reproduced successfully but with severe crack formation over the entire surface of “SU-8 50”. To mitigate this issue, crack annealing technique that was developed during process optimization runs was performed, which healed the surface and did not adversely affect the underlying “SU-8 5” and metal layers. The total thickness of the polymer-metal-polymer composite structure was measured and determined to be $\sim 70 \mu\text{m}$, indicating a thickness of $\sim 63 \mu\text{m}$ for the patterned “SU-8 50” layer, making it slightly higher than the minimum targeted thickness of $\sim 50 \mu\text{m}$ and providing added mechanical stability to the microelectrode structure (Fig. 4d).

Patterning of the gold layer to define the boundaries of each electrode and to open etch holes, followed by sacrificial layer etching to release the microelectrode structures were successfully performed (Fig. 4e and 4f). The tri-layer sandwiched microelectrode architecture remained intact upon release, owing to the special design of the etch holes in the “SU-8 50” layer which were patterned to have smaller openings than their counterparts in the “SU-8 5” layer and effectively served as mechanical locks holding together the multi-layer structure. Figure 5 shows optical microscope images of successfully fabricated devices both before and after release. With the developed microelectrode design and microfabrication process flow, both discrete electrodes and multi-electrode flexible strips were successfully realized. Once devices were released, they were tested with a multimeter for electrical continuity by touching the “contact pad” region on the top side created for external electrical routing, and the “sensing nodes” on the bottom side for interfacing with the skin or biological

tissue. The resistance of a 1x1 cm discrete electrode was measured to be less than 1 Ω . Based on the results, the developed process flow on 3 in. wafers was confirmed to be repeatable and offered very high yields above 90%.

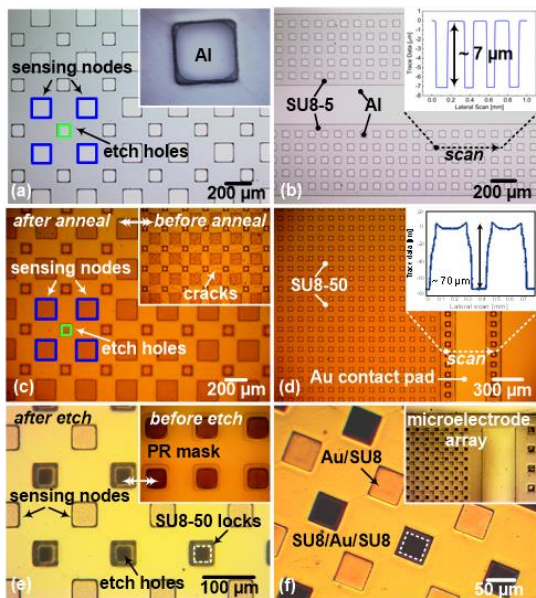


Figure 4 Optical microscope images of the fabricated flexible microelectrode pictured different instances during the process flow: (a-b) deposition of the sacrificial Al layer and patterning of the bottom “SU8-5” layer; (c-d) deposition of the structural gold layer and patterning of the top “SU8-5” layer; (e-f) creating the etch holes and sacrificial layer release

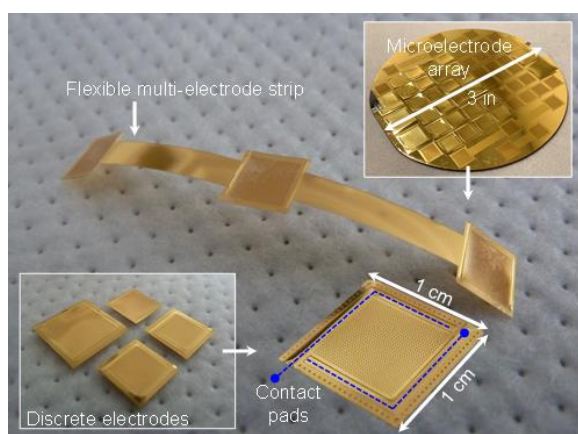


Figure 5 Optical microscope images of the fabricated multilayer flexible SU8-Au microelectrode arrays showing discrete electrodes as well as a flexible multi-electrode strip

3. APPLICATION TO WEARABLE HEALTH MONITORING

Monitoring, recording and processing of biopotential signals due to cardiac, neural or muscular activities constitute a large portion in wearable health applications. As the electrode is the main enabler of such applications, to demonstrate the functionality of the fabricated flexible multilayer micro electrodes, they were tested in an electrocardiogram (ECG) recording scenario.

Accordingly, thin electrical wires were first dipped into silver paste and then positioned inside the microelectrode’s “contact pad” region simply by insertion. Upon drying of the silver paste within approximately a minute, the wire was secured inside the contact pad, and this facilitated subsequent electrical interfacing of the microelectrode with external circuits or measurement instruments. Figure 6a shows, assembled microelectrodes that were successfully prepared following this protocol.

To acquire ECG signals a custom-made biopotential measurement system was used which included an analog front-end for signal amplification and on-board filtering, as well as a microcontroller and a Bluetooth module for signal digitization and wireless transmission to a remote graphical user interface (GUI). To construct the GUI, LabVIEW (National Instruments, NI) was used. LabVIEW is a commercially available visual programming tool based on usage of “block diagrams” and facilitates setting up of PC-based GUIs for instrumentation, measurement, and control.

Data packets sent via the Bluetooth module are accessed from the PC’s serial port upon optimizations such as adjusting the delays in the COM-Port settings low on the computer side and data transfer with a high baud rate (115200 pulse per second). This way, it was possible to increase the sampling frequency up to 2 kHz for the

measurements. The basic function of the code to implement the GUI is to continuously read the data packets coming to the serial port in a loop, to eliminate or suppress noise by passing the received waveform through digital band-pass filters constructed in these loops, and to eventually display the processed ECG waveform in real-time. By including suitable R-peak detection algorithms in the LabVIEW graphical coding environment it is also possible to show critical features like the heart rhythm in the constructed GUI.

Electrocardiogram recording experiments were performed on a 27-year old voluntary male participant with no reported health problems (studies were performed with the Sabanci University ethics committee approval no FENS-2020-48, and followed the protocols set forth in the Helsinki Declaration of 1975, as revised in 2013). The participant was instructed to sit in a relaxed position and maintain both arms in a stationary condition. Without any prior skin preparation, two microelectrodes, one on each wrist, were secured in place with the help of adhesive foam tape, while a reference electrode (Ag/AgCl) was placed further above on either of the arms for recording ECG in lead-I configuration (Figure 6b).

First, ECG from the stated location was acquired using silver/silver chloride electrodes to verify the circuit operation. Next, using the flexible microelectrodes, approximately one minute long electrocardiogram was recorded with clear representation of R-peaks (Figure 7a).

By utilizing Fast Fourier Transform (FFT) the recorded electrocardiogram was plotted in the frequency domain to evaluate the frequency content of the signal. As expected the signal largely resided below 40 Hz, which is typical of cardiac activity. Although minor, coupling of the 50 Hz powerline noise from the ambient was still apparent in the frequency spectra despite

the analog filtering. Such noise sources and potential artifacts due to motion are typical in wearable dry electrodes and can be eliminated using various strategies including discrete wavelet transform and digital filtering [24, 25].

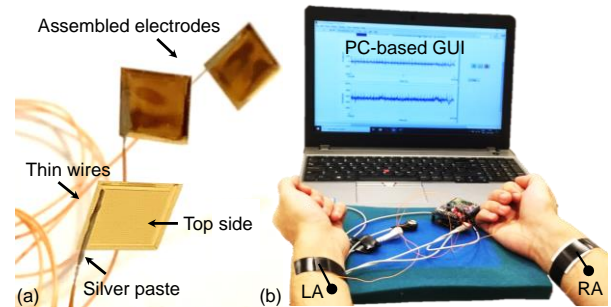


Figure 6 (a) Images of electrically interfaced microelectrodes; (b) experimental setup for ECG recording

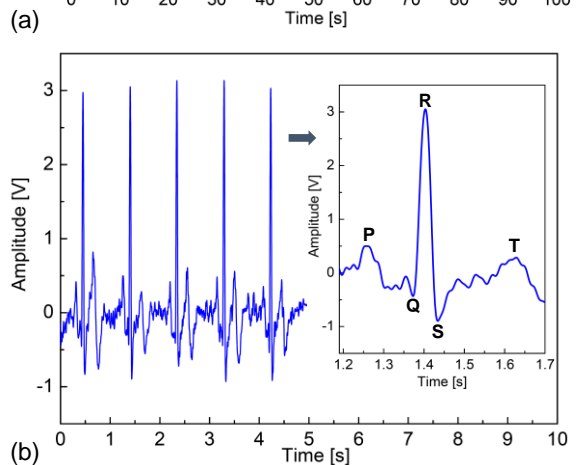
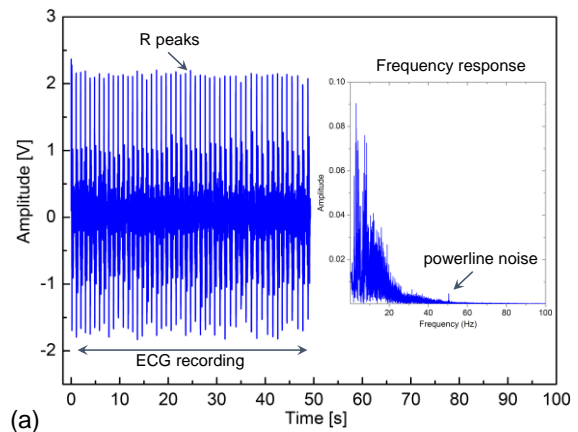


Figure 7 Electrocardiogram (ECG) recordings acquired with the flexible microelectrodes in lead-I configuration: (a) sample of a long ECG recording reaching one minute duration with visible R-peaks, inset shows the computed frequency response; (b) sample of a shorter ECG recording showing the P-QRS-T complex

Accordingly, a 5 second ECG recording obtained with the flexible microelectrodes was bandpass-filtered (1-49 Hz) which clearly revealed the clinically relevant P-QRS-T morphology (Figure 7b).

4. CONCLUSION

A key enabler of wearable applications is the gel-free, dry, skin-conformal bioelectrode. In this work, multilayer flexible microelectrode arrays were designed and fabricated. The novel design presented here allowed structuring of biocompatible SU8 and Au layers in a tri-layer sandwich architecture where an array of conformal sensing nodes were created in the plane directly contacting the skin. Through metal deposition on the positively sloped sidewalls of trenches, the sensing nodes were routed in the vertical direction away from the skin to a higher elevation. This unique approach provided seamless electrical interfacing through contact pads located atop the microelectrode without disturbing the contact conditions between the skin and the active, sensing side of the flexible microelectrode.

Optimized parameters concerning each step of the fabrication flow were systematically determined along with the development of a “crack anneal” process which allowed high-yield, repeatable and scalable microfabrication of flexible microelectrode arrays. The functionality of the fabricated flexible microelectrodes were demonstrated by successful acquisition of the electrocardiogram in lead-I configuration where critical cardiac signatures (i.e. P-QRS-T complex) were detected. The tri-layer composite SU8/Au microelectrode structure proved to offer seamless interfacing with peripheral electronics without interfering with the skin-electrode contact and this feature will be instrumental particularly towards the development of wearable applications and bioelectronics in the grand scheme.

Funding

This work was supported in part by the Faculty of Engineering and Natural Sciences, Sabanci University.

The Declaration of Conflict of Interest/ Common Interest

No conflict of interest or common interest has been declared by the authors.

The Declaration of Ethics Committee Approval

The experimental procedures involving volunteer human subjects described in this paper was approved by the Ethics Committee of Sabanci University (Sabancı Üniversitesi Araştırma Etik Kurulu, date: 9 Dec. 2020, form no: FENS-2020-48), and followed the principles outlined in the Helsinki Declaration of 1975, as revised in 2013. The participants gave their informed consent for inclusion before they participated in the study. The authors gratefully thank the participants involved in this study.

The Declaration of Research and Publication Ethics

The authors of the paper declare that they comply with the scientific, ethical and quotation rules of SAUJS in all processes of the paper and that they do not make any falsification on the data collected. In addition, they declare that Sakarya University Journal of Science and its editorial board have no responsibility for any ethical violations that may be encountered, and that this study has not been evaluated in any academic publication environment other than Sakarya University Journal of Science.

REFERENCES

- [1] C. Chitrakar, E. Hedrick, L. Adegoke, M. Ecker, “Flexible and stretchable bioelectronics,” *Materials*, vol. 15, no.5, pp. 1664, 2022.

- [2] S. Lee, J. Park, S. Kim, J. Ok, J. I. Yoo, Y. S. Kim, Y. Ahn, T-i. Kim, H. C. Ko, J. Y. Lee, "High-Performance implantable bioelectrodes with immunocompatible topography for modulation of macrophage responses," *ACS Nano*, vol. 16, no.5, pp. 7471–7485, 2022.
- [3] Z. Wang, H. Bai, W. Yu, Z. Gao, W. Chen, Z. Yang, C. Zhu, Y. Huang, F. Lv, S. Wang, "Flexible bioelectronic device fabricated by conductive polymer-based living material," *Science Advances*, vol.8, no.25, pp. eabo1458, 2022.
- [4] Y. Chen, Y. Zhang, Z. Liang, Yu Cao, Zhiyuan Han, Xue Feng, "Flexible inorganic bioelectronics," *npj Flexible Electronics*, vol.4, no.2, pp. 1-20, 2020.
- [5] L. Zhang, K. S. Kumar, H. He, C. J. Cai, X. He, H. Gao, S. Yue, C. Li, R.C-S. Seet, H. Ren, J. Ouyang "Fully organic compliant dry electrodes self-adhesive to skin for long-term motion-robust epidermal biopotential monitoring", *Nature Communications*, vol. 11, no. 4683, pp. 1-13, 2020.
- [6] D. H. Kim, N. Lu, R. Ma, Y. S. Kim, R. H. Kim, S. Wang, J. Wu, S. M. Won, H. Tao, A. Islam, K. J. Yu, T. I. Kim, R. Chowdhury, M. Ying, L. Xu, M. Li, H. J. Chung, H. Keum, M. McCormick, P. Liu, Y. W. Zhang, F. G. Omenetto, Y. Huang, T. Coleman, J. A. Rogers "Epidermal electronics," *Science*, vol. 333, no. 6044, pp. 838-843, 2011.
- [7] J. Viventi, D. H. Kim, J. D. Moss, Y. S. Kim, J. A. Blanco, N. Annetta, A. Hicks, J. Xiao, Y. Huang, D. J. Callans, J. A. Rogers, B. Litt "A conformal, bio-interfaced class of silicon electronics for mapping cardiac electrophysiology," *Science Translational Medicine*, vol. 2, no. 24, pp. 24ra22, 2010.
- [8] M. Ferguson, D. Sharma, D. Ross, F. Zhao, "A Critical Review of Microelectrode Arrays and Strategies for Improving Neural Interfaces," *Advanced Healthcare Materials*, vol.8, pp. 1900558, 2019.
- [9] S. Moussa, J. Mauzeroll, "Review—Microelectrodes: An Overview of Probe Development and Bioelectrochemistry Applications from 2013 to 2018," *Journal of the Electrochemical Society*, vol. 166, no. 6, pp. G25-G38, 2019.
- [10] T. I. Oh, S. Yoon, T. E. Kim, H. Wi, K. J. Kim, E. J. Woo, R. J. Sadleir, "Nanofiber web textile dry electrodes for long-term biopotential recording," *IEEE Transactions on Biomedical Circuits and Systems*, vol. 7, no. 2, pp. 204-211, 2013.
- [11] Y. Wang, Y. Qiu, S. K Ameri, H. Jang, Z. Dai, Y. A. Huang, N. Lu, "Low-cost, μm -thick, tape-free electronic tattoo sensors with minimized motion and sweat artifacts," *npj Flexible Electronics*, vol.2, no.6, 2018.
- [12] G. Paul, R. Torah, S. Beeby, J. Tudor, "The development of screen printed conductive networks on textiles for biopotential monitoring applications," *Sensors and Actuators A: Physics*, vol.206, pp. 35–41, 2014.
- [13] F. Stauffer, M. Thielen, C. Sauter, S. Chardonnens, S. Bachmann, K. Tybrandt, C. Peters, C. Hierold, J. Vörös, "Skin Conformal Polymer Electrodes for Clinical ECG and EEG Recordings," *Advanced Healthcare Materials*, vol. 7, pp. 1700994, 2018.

- [14] M. A. Yokus, T. Songkakul, V. A. Pozdin, A. Bozkurt, M. A. Daniele, "Wearable multiplexed biosensor system toward continuous monitoring of metabolites," *Biosensors and Bioelectronics*, vol. 153, pp. 12038, 2020.
- [15] N. X. Williams, A. D. Franklin, "Electronic Tattoos: A Promising Approach to Real-time Theragnostics," *Journal of Dermatology and Skin Science*, vol. 2, 1, pp. 5-16, 2020.
- [16] C. Wang, K. He, J. Li, X. Chen, "Conformal electrodes for on-skin digitalization," *SmartMat*, vol.2, pp.252-262, 2021.
- [17] J. Alberto, C. Leal, C. Fernandes, P. A. Lopes, H. Paisana, A. T de Almeida, M. Tavakoli, "Fully Untethered Battery-free Biomonitoring Electronic Tattoo with Wireless Energy Harvesting," *Scientific Reports*, vol.10, no. 5539, pp. 1-11, 2020.
- [18] B. F. E. Matarèse, P. L. C. Feyen, A. Falco, F. Benfenati, P. Lugli, J. C. DeMello, "Use of SU8 as a stable and biocompatible adhesion layer for gold bioelectrodes," *Scientific Reports*, vol. 8, no. 5560, pp.1-12, 2018.
- [19] H. Lorenz, M. Despont, N. Fahrni, N. LaBianca, P. Renaud, P. Vettiger, "SU-8: a low-cost negative resist for MEMS," *Journal of Micromechanics and Microengineering*, vol. 7, no. 3, pp.121-4, 1997.
- [20] T. A. Anhoj, A. M. Jorgensen, D. A. Zauner, Jörg Hübner, "The effect of soft bake temperature on the polymerization of SU-8 photoresist," *Journal of Micromechanics and Microengineering*, vol. 16, pp. 1819, 2006.
- [21] R. Feng, R. J. Farris, "Influence of processing conditions on the thermal and mechanical properties of SU8 negative photoresist coatings," *Journal of Micromechanics and Microengineering*, vol.13, no. 1, pp. 80-88, 2003.
- [22] S. Keller, G. Blagoi, M. Lillemose, D. Haefliger, A. Boisen, "Processing of thin SU-8 films", *Journal of Micromechanics and Microengineering*, vol. 18, pp. 125020, 2008.
- [23] G. Hass, J. E. Waylonis, "Optical Constants and Reflectance and Transmittance of Evaporated Aluminum in the Visible and Ultraviolet," *Journal of the Optical Society of America*, vol. 51, pp. 719-722, 1961.
- [24] S. Banerjee, R. Gupta, M. Mitra, "Delineation of ECG characteristic features using multiresolution wavelet analysis method," *Measurement*, vol. 45, no. 3, pp. 474-487, 2012.
- [25] S. Asgari, A. Mehrnia, "A novel low-complexity digital filter design for wearable ECG devices," *PLoS One*, vol.12, no. 4, pp. e0175139, 2017.